Hail detection using S and C band radar reflectivity difference

Laurent Féral, Henri Sauvageot, Serge Soula

▶ **To cite this version:**

Laurent Féral, Henri Sauvageot, Serge Soula. Hail detection using S and C band radar reflectivity difference. Journal of Atmospheric and Oceanic Technology, 2003, 20, pp.233-248. 10.1175/1520-0426(2003)0202.0.CO;2 . hal-00136467

HAL Id: hal-00136467
https://hal.science/hal-00136467v1

Submitted on 23 Feb 2023

HAL is a multi-disciplinary open access archive for the deposit and dissemination of scientific research documents, whether they are published or not. The documents may come from teaching and research institutions in France or abroad, or from public or private research centers.

L'archive ouverte pluridisciplinaire **HAL**, est destinée au dépôt et à la diffusion de documents scientifiques de niveau recherche, publiés ou non, émanant des établissements d'enseignement et de recherche français ou étrangers, des laboratoires publics ou privés.

Distributed under a Creative Commons Attribution 4.0 International License

Hail Detection Using S- and C-Band Radar Reflectivity Difference

LAURENT FÉRAL

ONERA-CERT, Département Electromagnétisme et Radar, Toulouse, France

HENRI SAUVAGEOT AND SERGE SOULA

Université Paul Sabatier, Observatoire Midi-Pyrénées, Laboratoire d'Aérologie, Toulouse, France

(Manuscript received 13 March 2002, in final form 15 August 2002)

ABSTRACT

In reflectivity fields observed with conventional radar networks, hailstorm identification is not easy. In the present paper, a hailstorm detection method using two single-wavelength radars located far from each other is discussed. The two radars, C and S bands, respectively, are about 200 km apart. Because large hailstones are non-Rayleigh scatterers, the distribution of the dual-wavelength reflectivity ratio is shown to display an identifying signal for hail-bearing storms. The relevance and sensitivity of the proposed hail detection algorithm is first analyzed from a simulation of 10.7- and 5.3-cm radar observations. Various convective storm conditions, differing by the horizontal shape and the nature of precipitation, are considered, notably rain and hail with hailstones of different diameters, dry or coated with liquid water. The attenuation for the radar–target propagation path and inside the target is also taken into account. The dual-wavelength reflectivity ratio for all the simulated radar observations shows that the proposed criterion enables an identification of the hail-bearing storms. The algorithm is then applied to real cases of storms observed with the French meteorological radar network. The comparison of the hail areas identified by the dual-wavelength algorithm with the hail impacts observed with ground-based hailpad networks confirms the ability of the algorithm to detect the hail-bearing cells in proper time and place. It is concluded that the dual-wavelength reflectivity ratio has a potential for hail detection, using an operational radar network organized in such a way that the convective field can be simultaneously observed with both an S-band and a C-band radar.

1. Introduction

Starting with the pioneering attempts of Byers and Braham (1949), many works have tried to detect hail-bearing cells inside convective storms. This type of information is useful to short-term forecasting, to a correct interpretation of the radar reflectivity in terms of precipitation rate at the ground, to an improved knowledge of the precipitation processes in convective clouds, and for hydrological purposes.

Hail development processes have not yet been completely understood and the problem of hail prediction at the scale of the individual convective storm has not been solved, which makes radar observation very important. Hailfall covers a wide intensity spectrum and its spatiotemporal distribution inside convective complexes is very heterogeneous. At midlatitudes, over continents, hail occurrence at the ground is rather common and the violent and damaging hailstorms represent only a very low percentage of the total. For example, in southwestern France, where hail damage is rather high, less than 1% of the hailstorms are damaging though they are large hailstone producers (Dessens 1986; Vinet 2001). The storms generating the large and damaging hailstones are, of course, the more useful to detect. Hail develops inside the storms in the form of discontinuous and possibly pulsatory hailstreaks (Changnon 1970; Kessler 1983; Young 1993).

Hail detection with a single wavelength conventional radar is not straightforward. Because hailstones lie outside the Rayleigh scattering region, at current radar wavelengths, there is no simple relationship between the size of the scatterers and the backscattered intensity. The electromagnetic Mie scattering resonance, the surface condition (dry or wet), and the hailstone texture, but also the small horizontal extent of the hailstreaks, possibly less than the width of the radar beam, increase the confusion.

Various methods and algorithms have been proposed to identify the presence of hail in storms by radar. Reviews can be found in Kessler (1983) or Atlas (1990). For example, hail identification criteria using the vertical profile of the radar reflectivity have been suggested; the maximum value of the equivalent radar reflectivity

Corresponding author address: Dr. Laurent Féral, Onera-Cert, Département Electromagnétisme et Radar, BP 4025, 2 avenue Edouard Belin, 31055 Toulouse Cedex 4, France.
E-mail: laurent.feral@onera.fr

© 2003 American Meteorological Society

Unauthenticated | Downloaded 02/23/23 09:20 AM UTC

factor aloft, $Z_{e\max}$, and the ratio of this quantity to the value of Z_e at ground level increase with the intensity of the convective storm and the probability of hailfall. Taken together, the results obtained for hail detection from criteria based on threshold reflectivity values and/or on a particular form of the echo structure (e.g., hook echo) confirm that, although useful, the single-wavelength reflectivity measurements contain a large amount of uncertainty. Moreover, this approach is pertinent only for S-band radars (wavelength $\lambda = 10$ cm), because of the size of the first Mie mode (about 3 cm), and in the absence of attenuation, since attenuation can be very significant even at S band when observing through convective storms.

A hail signal can be obtained with the joint measurement of Z_e and of a parameter of polarization. Indeed, the hailstones gyrate when falling, so that, in spite of their nonspherical shapes (responsible for their behavior in circular polarization), hail precipitation presents no preferential orientation and the values of the differential reflectivity Z_{DR} they produce are close to zero. Rain is characterized by $Z_{\mathrm{DR}} > 0.5$ dB and an equivalent radar reflectivity factor that can reach about 57 dBZ. Thus, in a region of high reflectivity associated with the intense precipitation of convective storms, the high values of Z_{DR} are due solely to the rain, whereas the weak or equal to zero values of Z_{DR} show the presence of hail. When there is a mixture of rain and hail, the contribution of the hail is supposed to prevail over that of the rain, because of the size of the hailstones. The Z_{DR} signature of the hail is easily identifiable below the melting level. However, this method is spoiled by differential attenuation between horizontal and vertical polarization; it is thus usable only at S band (Bringi et al. 1986; Illingworth et al. 1987; Sauvageot 1996; Kennedy et al. 2001). Besides that, operational radar networks do not have the polarization diversity ability. That is why it is useful to consider alternative methods for hail detection.

The use of the reflectivity dependence on the wavelength in the Mie scattering region to detect the hail from simultaneous observations with a dual-wavelength radar (i.e., two collocated radars using colinear antenna beams) was first proposed by Atlas and Ludlam (1961). Since they are different, these two wavelengths are attenuated differently. If $Z_m(r)$ is the logarithm of the radar reflectivity factor observed at distance r along the radar beam, it may be defined as follows:

$$Z_{m\alpha}(r) = Z_\alpha(r) - 2\int_0^r a_\alpha(r)\, dr, \qquad (1)$$

where $Z_\alpha(r)$ is the equivalent radar reflectivity factor that would be observed in the absence of attenuation and $a(r)$ is the attenuation coefficient that combines all the attenuation causes (gas, cloud, rain, hail). Subscript $\alpha = l$ corresponds to the longest wavelength λ_l and $\alpha = s$ to the shortest one λ_s. The parameter of interest in the dual-wavelength methods is the dual-wavelength ratio (DWR) $= y(r) = Z_{ml}(r) - Z_{\mathrm{ms}}(r)$; that is,

$$y(r) = [Z_l(r) - Z_s(r)] - \int_0^r a_l(r) - a_s(r)]\, dr. \qquad (2)$$

In the Rayleigh scattering conditions, $Z_l(r) = Z_s(r)$ and the radial variation of $y(r)$ depends only on the cumulative differential attenuation $A_d(r)$ represented by the integral on the right-hand side of (2). In the presence of non-Rayleigh scatterers, $Z_l \neq Z_s$ and the reflectivity difference, that is, the first term in the bracket, on the right-hand side of (2) is not zero. This bracket is a non-Rayleigh term.

The DWR is used in two kinds of methods according to the scattering conditions, which depend on the size of the scatterers and on the choice of the wavelengths.

Using the measurement Δy of the DWR difference between two volumes of the radar beam $V(r)$ and $V(r + \Delta r)$, separated by a range increment Δr has been proposed, to retrieve, from the ΔA_d variation, the rain- or cloud water content integrated along Δr (Atlas 1954; Eccles and Mueller 1971; Eccles and Atlas 1973; Atlas and Ulbrich 1974; Gosset and Sauvageot 1992; Vivekanandan et al. 1999). Of course, non-Rayleigh scatterers inside the volumes $V(r)$ and $V(r + \Delta r)$ used to compute $\Delta y(r)$ can jeopardize these methods because the difference between Z_l and Z_r creates an ambiguity about the cause of Δy variations (the presence of non-Rayleigh scatterers between the two volumes does not). The pair of wavelengths is, in this case, chosen at the best trade-off in order to minimize the non-Rayleigh term and to maximize the differential attenuation term.

The wavelength pair can also be selected in order to make the non-Rayleigh term significant in order to use it to size the scatterers. For example, the use of the wavelength pair 10–3 cm (S and X bands, respectively) has been proposed for hail (Atlas and Ludlam 1961; Eccles and Atlas 1973), and that of the wavelength pair 0.86–0.32 cm (K_a and W bands, respectively) for cirrus ice crystals (Hogan et al. 2000).

In the case of hail, which is the subject of the present paper, the dual-wavelength ratio depends on other factors than the size, notably the physical state (dry or wet) of the hailstone surface, the homogeneity of the target with respect to the size of the corresponding beams at the two wavelengths, and so on. The method proposed by Eccles and Atlas (1973) eliminates certain defects associated with the direct use of the equivalent radar reflectivity factor. It uses the derivative with respect to the distance $dy(r)/dr$ and the wavelength pair 10–3 cm, in such a way that a_l is negligible compared to a_s in (2). In rain $Z_l \approx Z_s$ and $y(r)$ increases in a monotonic manner with r. If hail precipitation with diameters larger than 1 cm is present in the beam, y increases more rapidly at the front of the hail volume and decreases at the rear because hailstones have a much larger backscattering cross section at 10 cm than at 3 cm ($Z_{10} \gg$

Unauthenticated | Downloaded 02/23/23 09:20 AM UTC

Z_3). In the absence of hail, dy/dr expresses the attenuation coefficient at 3 cm. In the presence of hail, it has a sharp variation, positive at the front of the hail zone, small or negative at the rear of the hail zone. Whereas the positive variation of dy/dr can be attributed to attenuation by a region of high water content, the negative value can be due only to large size hail. The authors therefore suggest considering the negative value as an indicator that unequivocally locates the rear boundary of a hail zone. Because only a small ratio of radar reflectivity is required at two wavelengths, the technique is not affected by the attenuation and is independent from the absolute calibration of the radars. However, the method presents difficulties concerning the coincidence of the beams relative to each wavelength (Rinehart and Tuttle 1982), attenuation differences (Tuttle and Rinehart 1983), and measurements simultaneousness. A negative value of dy/dr indicates the presence of hail with size larger than 1 cm. However, it is not a sure indication of the farthest boundary of the hail zone and can be produced within a region where the size of the hail, or the thickness of the water film surrounding the hailstone, varies with distance (Jameson and Srivastava 1978). In conclusion, the inconvenience of this method is the technical difficulty in obtaining measurements having the necessary accuracy and a lack of clarity in the hail signal. Moreover, all the dual-wavelength methods discussed above use a dual-wavelength radar system, that is, two collocated radars, usually set up on a common pedestal. There is no such radar system in radar networks.

The aim of the present paper is to propose a dual-wavelength method for hail detection using two individual radars working at C and S bands (5.3 and 10.7 cm, respectively), located far from each other. Areas observed simultaneously by two meteorological radars working at C and S bands are frequent in the operational networks, for example, in France and United States. The method is discussed from a simulation, in order to test the sensitivity to the radar and target parameters, and from field data.

2. Hail detection method

In order to identify the hail areas, the computation of a dual-wavelength reflectivity ratio from two radars distant from each other is proposed. Because the Mie effects and the radar–target distances are different from one radar to the other, for each term of the ratio, it is not the direct radar reflectivity factor that is used but the ratio of the mean reflectivity over the hail area $\langle Z_{\text{Hail}} \rangle$ to the mean reflectivity over the surrounding rainy area $\langle Z_{\text{Rain}} \rangle$. Processing locally, with relative values, enables one to avoid biases depending on the radar characteristics and on the radar–target propagation conditions.

Let us consider a hailstorm observed with two radars, one S band and the other C band, located far from each other. These radars are assumed to be correctly aligned and providing correct ranges. Each radar provides plan position indicator (PPI) images of the storm every 5 min in the form of Cartesian images with a uniform pixel size of 1 km $\times$ 1 km. Two PPIs provided by each of the two radars almost at the same time (i.e., at $t \pm 1$ min) are used.

The PPI image of the 10-cm radar is thresholded at a value $\tau_1 = 40$ dBZ (equivalent to about 10 mm h^{-1} using the standard Z–R relation $Z = 300\,R^{1.5}$, with Z in mm^6 m^{-3} and R in mm h^{-1}, relation representative for the convective storms in France) that is significantly lower than the reflectivity of the highest peaks usually observed in convective storms. This thresholding enables the selection of N (≥ 0) rain areas $(A^{10\text{cm}}_{40\text{dB}Z})_{i=1,\ldots,N}$ in the PPI.

For each $(A^{10\text{cm}}_{40\text{dB}Z})_{i=1,\ldots,N}$, the maximum reflectivity $Z_{\max}$ is used to define a second threshold $\tau_2 = Z_{\max} - 3$ dB. Threshold τ_2 enables the isolation inside each $A^{10\text{cm}}_{40\text{dB}Z}$ of a single heavy area assumed to deserve to be tested as hail area. This area is labeled $A^{10\text{cm}}_{\text{Hail}}$. Its mean reflectivity value $\langle Z^{10\text{cm}}_{\text{Hail}} \rangle$ is computed.

A rainy area $A^{10\text{cm}}_{\text{Rain}}$ is defined as the area of a 3-km-wide band spreading outside the τ_1 contour. The value 3 km has been empirically chosen. As an example, Fig. 1 illustrates the definitition of the diverse areas (see also section 4). The mean reflectivity $\langle Z^{10\text{cm}}_{\text{Rain}} \rangle$ inside $A^{10\text{cm}}_{\text{Rain}}$ is computed.

Each area $A^{10\text{cm}}_{40\text{dB}Z}$ defined from the 10-cm radar has to be identified on the corresponding 5-cm PPI. As the propagation conditions and the technical characteristics are different from one radar to the other, the spatial identification of the areas cannot be achieved by simply applying the previous threshold value $\tau_1 = 40$ dBZ. Indeed, the best spatial agreement is obtained by combining area criterion and successive thresholdings. That is why the corresponding 5-cm PPI image is thresholded until the area, $A^{5\text{cm}}$, is as close as possible to the $A^{10\text{cm}}_{40\text{dB}Z}$ under consideration, that is, $A^{10\text{cm}}_{40\text{dB}Z} \sim A^{5\text{cm}}$. Then each $A^{5\text{cm}}$ area is thresholded from its local maximum reflectivity value to its minimum value. By doing this, several subareas are eventually defined. Among these, the hail area, $A^{5\text{cm}}_{\text{Hail}}$, is the one having an area as close as possible to $A^{10\text{cm}}_{\text{Hail}}$ while minimizing the intercentroid distance between $A^{10\text{cm}}_{\text{Hail}}$ and $A^{5\text{cm}}_{\text{Hail}}$. The hail area mean reflectivity value, $\langle Z^{5\text{cm}}_{\text{Hail}} \rangle$, is then computed. Proceeding this way, the hail areas observed by the 5-cm wavelength radar are not necessarily the areas where the mean reflectivity value is maximum, in compliance with the results of Atlas and Ludlam (1961). As for the 10-cm image, $A^{5\text{cm}}_{\text{Rain}}$ area is defined as the 3-km-wide band surrounding the $A^{5\text{cm}}$ area and the $\langle Z^{5\text{cm}}_{\text{Rain}} \rangle$ is computed (Fig. 1).

In order to evaluate the spatial agreement between the hail areas and the rain areas, two criteria are suggested. First, the centroid coordinates of $A^{10\text{cm}}_{\text{Hail}}$ are computed with respect to the 10-cm radar and with respect to the 5-cm radar. Then, the intercentroid distance D_{IB} between $A^{10\text{cm}}_{\text{Hail}}$ and $A^{5\text{cm}}_{\text{Hail}}$ is obtained. Second, to appreciate

Unauthenticated | Downloaded 02/23/23 09:20 AM UTC

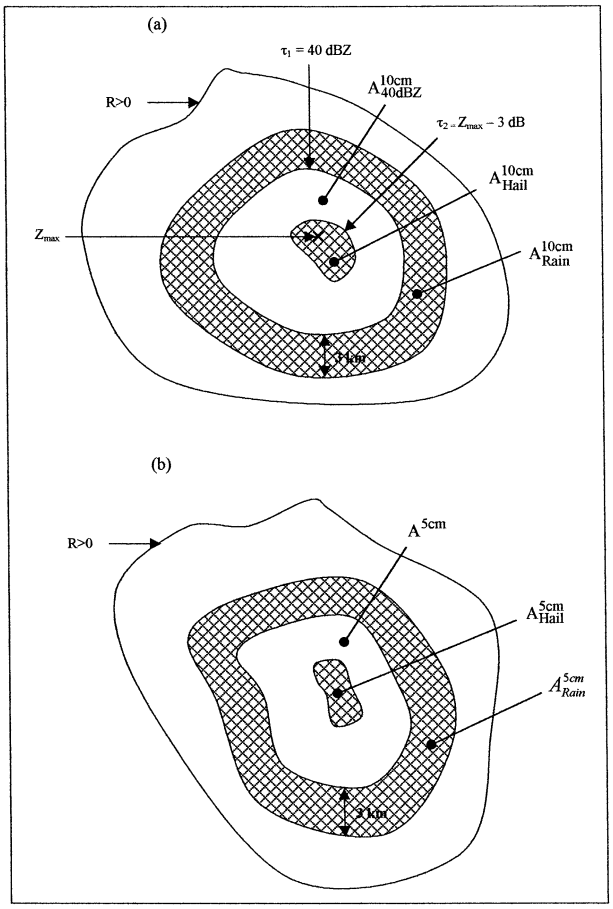

FIG. 1. Definition of the diverse radar areas (a) from the S-band and (b) from the C-band radar. The outer boundary of the rain area is $R > 0$.

the degree of spatial coincidence between the rainy areas, the coordinates of the pixels defining the rainy area $A_{\text{Rain}}^{10\text{cm}}$ with respect to the 10-cm radar are computed with respect to the 5-cm radar. Then, the number of pixels shared by the two rainy areas $A_{\text{Rain}}^{10\text{cm}}$ and $A_{\text{Rain}}^{5\text{cm}}$ is obtained. This number is turned into a percentage P_{SC} with respect to the $A_{\text{Rain}}^{10\text{cm}}$ total number of pixels. Finally, the spatial agreement criterion is said to be verified when the two following conditions are fulfilled:

1) $D_{\text{IB}} < 5$ km and
2) $P_{\text{SC}} > 50\%$.

For each rain area seen by the two radars, one can then compute a dual-wavelength reflectivity hail ratio (DWHR) defined as

$$\text{DWHR} = 100\frac{\langle Z_{\text{Hail}}^{10\text{ cm}}\rangle/\langle Z_{\text{Rain}}^{10\text{ cm}}\rangle}{\langle Z_{\text{Hail}}^{5\text{ cm}}\rangle/\langle Z_{\text{Rain}}^{5\text{ cm}}\rangle}, \quad (3)$$

with DWHR in percent.

Among the areas that agree with the two previous constraints, the hail-bearing areas now have to be determined. Theoretically a rain area made up of only liquid precipitation, that is, composed of Rayleigh scatterers, should have a DWHR equal to 100%, while the hail-bearing areas, due to the differences between the 10- and 5-cm reflectivity factors, should display a DWHR value higher than 100%. But how do DWHRs behave in real cases, that is, in the presence of different attenuation and beam averaging from one radar to the other? What is the sensitivity of the DWHR to define unequivocally the presence or absence of hail? To discuss these points a numerical simulation is proposed.

3. Numerical simulation

a. Meteorological target definition

In order to simulate the radar observations, the three-dimensional structure and the successive locations (with respect to the radars) of convective storms (or targets) have to be specified. Three different shapes of horizontal cross sections are considered for the storms, one circular and two rectangular, with the large dimension oriented north–south for one and east–west for the other. As can be observed from PPI images and as mentioned by many authors, the typical horizontal cross section of a storm is composed of concentric areas over which the precipitation rate decreases from the center to the periphery. Consequently, the horizontal cross section of the simulated targets is made up of circular or rectangular concentric areas.

For each target shape, hail and no-hail cases are considered so that, finally, the number of simulated targets reaches six. The hail-bearing areas are modeled by a central hail core surrounded by three concentric rainy areas, the sizes and precipitation rates of which are specified in Table 1. The size of the hail area is defined according to Changnon's (1970) results on hailstreaks. The areas producing only rain are modeled by six con-

TABLE 1. Size and precipitation type for the concentric domains describing the horizontal section of the simulated hail-bearing areas. X and Y stand for zonal and meridional direction, respectively.

Precipitation type	Circular target diameter (km)	Rectangular target east–west axis (km)		Rectangular target north–south axis (km)	
		ΔX	ΔY	ΔX	ΔY
Hail	4	4.5	2.75	2.75	4.5
Rain of 40 mm h^{-1}	6	6.5	4.5	4.5	6.5
Rain of 10 mm h^{-1}	10	10.5	7.5	7.5	10.5
Rain of 2 mm h^{-1}	18	18.5	13.75	13.75	18.5

Unauthenticated | Downloaded 02/23/23 09:20 AM UTC

TABLE 2. Same as Table 1 but for the simulated rain areas.

Rain rate	Circular target diameter (km)	Rectangular target east–west axis (km)		Rectangular target north–south axis (km)	
		ΔX	ΔY	ΔX	ΔY
100 mm h^{-1}	1	1.5	0.5	0.5	1.5
80 mm h^{-1}	2	2.5	1.25	1.25	2.5
60 mm h^{-1}	4	4.5	2.75	2.75	4.5
40 mm h^{-1}	6	6.5	4.5	4.5	6.5
10 mm h^{-1}	10	10.5	7.5	7.5	10.5
2 mm h^{-1}	18	18.5	13.75	13.75	18.5

centric areas, the sizes and rain rates of which are specified in Table 2, following the description given by Browning et al. (1976) for the multicell storm observed at Raymer, Colorado. Considering hail-bearing and heavy rain targets will allow us to quantify the ability and the sensitivity of the algorithm for hail detection, while the three kinds of horizontal cross sections will account for the influence of the radar beam averaging according to distance. Figure 2 shows the horizontal cross sections of the six meteorological targets considered in the simulations. The target vertical structure is taken to be uniform.

The two radars are assumed to be 200 km apart, along an east–west baseline. This distance is similar to the mesh of operational radar networks. The targets are supposed to move along a line parallel to the radars' baseline but 50 km apart (below). The target centroids move on this line by 20-km steps defining 11 positions between 0 and 200 km, so that, at the beginning, the target is exactly 50 km below the first radar (S band, $X = 0$ km, $Y = 50$ km) to end 50 km below the second one (C band, $X = 200$ km, $Y = 50$ km). Figure 3 represents the location of the two radars and the successive positions of the target centroids considered in the simulations.

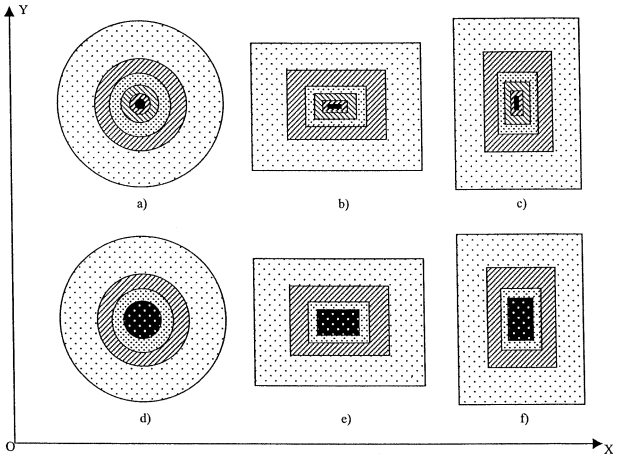

FIG. 2. Shape of the horizontal cross sections of the three kinds of modeled rainy targets: (a) circular, (b) rectangular east–west, and (c) north–south from left to right, respectively. In the six concentric areas, the precipitation rates are 100, 80, 60, 40, 10, and 2 mm h^{-1} from the center to the periphery, respectively. (d), (e), (f): Same as (a), (b), and (c) but for the hail cases. The central area is the hail; it is surrounded by the three concentric regions over which the precipitation rates are equal to 40, 10, and 2 mm h^{-1} successively. Axis OY points toward north.

b. Scatterer size distribution

The drop size distribution inside each region is modeled by an exponential function, namely,

$$N(D) = N_o \exp(-\Lambda D), \tag{4}$$

with $N_o = 0.08$ and $\Lambda = 41R^{-0.21}$ (Marshall and Palmer 1948). Here $N(D)$ and N_o are in cm^{-4}, Λ in cm^{-1}, D in cm, and R in mm h^{-1}. The term N is the number of drops per cubic centimeter per class of diameter. In the simulation, a size interval ΔD equal to 0.01 cm is considered, as well as a maximum drop diameter of 0.5 cm so that 50 classes of diameters, centered on the successive diameter values $(D_i)_{i=1...50} = \{0.005$ cm, 0.015 cm, . . . , 0.485 cm, 0.495 cm$\}$, are defined.

The hailstones' population is modeled in terms of dry and wet ice spheres. Considering a concentration $M = 1$ g m^{-3} of spherical hailstones and taking an ice density $\rho = 0.92$ g cm^{-3}, the concentration of hailstones with diameter D per unit volume is $6M/(\pi D^3\rho)$. In the simulations, D is successively equal to 2, 2.5, 3, 3.5, 4, and 4.5 cm. The hail population is made up of 50% of dry hailstones and 50% of wet hailstones. For wet hailstones, 35% and 15% are covered with a water shell 0.01 and 0.05 cm thick, respectively. These three hailstone percentages are written $P_{\mathrm{Hd}} = 50\%$, $P_{\mathrm{H0.01}} = 35\%$, and $P_{\mathrm{H0.05}} = 15\%$. Moreover, the hail volume is assumed

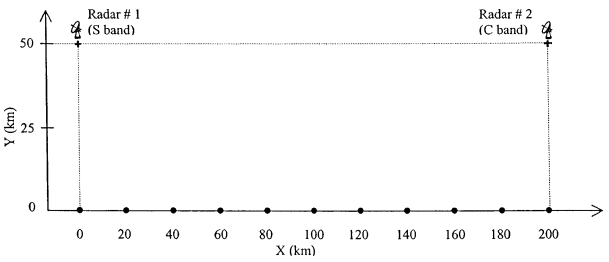

FIG. 3. Location in the horizontal plane of the two radars (+) and successive locations (X) of the target centroid (●) used in the simulations.

Unauthenticated | Downloaded 02/23/23 09:20 AM UTC

to be a mixing of hail and rain in the proportion of 50% of each. The rain component has a rate of 100 mm h^{-1}.

The main reason to use a monodisperse size distribution for hail is that the goal of the simulation is to determine the hail size that can effectively be detected with the proposed method. Second, observations at ground with the hailpad frequently show that instantaneous hailfall are monodisperse, the spectra only appearing when integrating in time or space.

c. Backscattering and attenuation cross sections

It is well known that the backscattering (σ) and attenuation (Q) cross sections of a spherical scatterer are given by the Mie formulas, the coefficient of which can be computed with the algorithm of Deirmendjian (1969). These coefficients depend on the radar wavelength λ, on the spherical diameter of the scatterer, and on its complex index of refraction. This latter is different for ice and for water. Assuming that both water and ice temperatures are 0°C, the Ray (1972) model is used to compute the complex index of refraction of scatterers. One can easily compute the backscattering and attenuation cross sections of all the hydrometeors under consideration in the simulation, that is, $(\sigma_i)_{i=1...50}$ and $(Q_i)_{i=1...50}$ for the homogeneous spherical drops of diameter $(D_i)_{i=1...50}$ constituting the six rainy regions, and σ_{Hd} and Q_{Hd} for the dry ice spheres of diameter D constituting 50% of the hailstones in the hail region. Figure 4a displays the equivalent reflectivity factor Z_e and Fig. 4b the two-way attenuation coefficient generated by a concentration of 1 g m^{-3} of dry spherical hailstones of uniform size as a function of the diameter for the wavelengths 5.3 and 10.7 cm.

Aden and Kerker (1951) gave a solution for the computation of the backscattering and attenuation cross sections of plane electromagnetic waves by an ice sphere with a concentric liquid water spherical shell. Their solution is general and, under appropriate conditions, reduced to the well-known solution of scattering from a homogeneous sphere. The backscattering ($\sigma_{\mathrm{H0.01}}$, $\sigma_{\mathrm{H0.05}}$) and attenuation ($Q_{\mathrm{H0.01}}$, $Q_{\mathrm{H0.05}}$) cross sections of ice spheres of diameter D coated with a layer of water equal to 0.01 and 0.05 cm, which are assumed to represent 35% and 15%, respectively, of the hailstone population, were thus computed. Table 3 gives the normalized attenuation cross sections of dry and coated ice spheres for various values of D and shell water thickness τ. Table 4 gives the one-way attenuation coefficients (dB km^{-1}) produced by ice spheres of uniform size for an ice mass of 1 g m^{-3}. The values reported in Tables 3 and 4 are in good agreement with those computed by Battan (1971). They show that attenuation cross sections and attenuation coefficients are much smaller for a 10.7- than for a 5.3-cm wavelength, except for $\tau = 0.05$ cm where the value for $\lambda = 10.7$ cm is similar or slightly higher than that for $\lambda = 5.3$ cm. Figures 5a and 5b show the equivalent reflectivity factor and the two-way attenuation coefficient as a function of the diameter D of the spherical hailstones for the modeled precipitation, that is, for a mixing of half of the water content in the form of rain, with a precipitation rate of 100 mm h^{-1}, and the other half in the form of hailstones, 50% of which are dry and 35% and 15% are coated with a water shell thickness of 0.01 and 0.05 cm, respectively. Figure 5c shows the reflectivity differences (attenuation included) between the two wavelengths corresponding to the observation of the mixed precipitation.

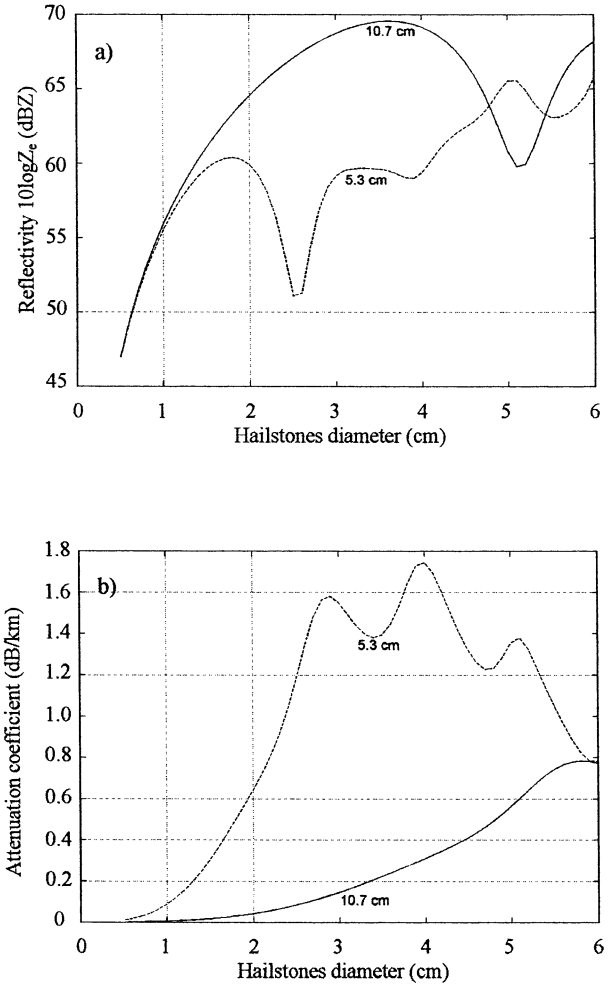

FIG. 4. (a) Reflectivity in dBZ and (b) two-way attenuation coefficient in dB km^{-1} for a concentration of 1 g m^{-3} of dry spherical hailstones of uniform size as a function of the diameter. The two wavelengths considered are 5.3 and 10.7 cm.

d. Equivalent radar reflectivity factor

The average power backscattered by a population of particles homogeneously distributed in an elementary pulse volume V is proportional to their radar reflectivity η, that is, to the sum of the backscattering cross sections (σ_i) of the individual particles, namely, $\eta = V^{-1} \Sigma_V \sigma_i$. Here η is commonly expressed in cm^{-1}. When the ob-

Unauthenticated | Downloaded 02/23/23 09:20 AM UTC

TABLE 3. Normalized attenuation cross sections of dry and coated ice spheres. The radar wavelength is λ, D the sphere diameter, τ the water shell thickness, and $\tau = 0.00$ is for dry hailstones.

	Sphere diameter (D, cm)																	
	2.0			2.5			3.0			3.5			4.0		
τ (cm)	0.00	0.01	0.05	0.00	0.01	0.05	0.00	0.01	0.05	0.00	0.01	0.05	0.00	0.01	0.05
λ (cm)															
5.3	0.909	2.685	2.948	2.079	3.387	2.967	3.283	3.858	3.000	3.446	4.309	2.757	4.928	4.257	3.058
10.7	0.060	0.224	1.112	0.150	0.391	2.706	0.312	0.657	3.896	0.557	1.070	3.648	0.882	1.726	3.557

served scattering volume does not satisfy the conditions of the Rayleigh approximation, which is the case for hailstones, or if there is any doubt that it does, it is convenient to characterize the radar reflectivity factor Z by the equivalent radar reflectivity factor Z_e, which is equal to the radar reflectivity factor of a population of spherical particles satisfying the Rayleigh approximation and producing a signal of the same power (e.g., Atlas 1990; Sauvageot 1992):

$$Z_e = \frac{\eta}{2.8 \times 10^{-10}\lambda^{-4}}, \tag{5}$$

with η in cm^{-1}, λ in cm, and Z_e in mm^6 m^{-3}. The radar reflectivity factor is usually expressed in dBZ; that is, $Z_e(\text{dBZ}) = 10 \log[Z_e \text{ (mm}^6 \text{ m}^{-3})]$.

e. Radar beam modeling and meshing

The characteristics of the two radars considered in the simulation, a 10.7- and a 5.3-cm wavelength radar, are the same as the radars of the French operational radar network (Table 5). The radar beam is modeled by a cone of aperture equal to the 3-dB beamwidth ($\theta_{3\text{dB}}$). The range bins, defining the resolution volumes, are 500 m from each other. When the radar beam intercepts the target, for each resolution volume, the radar reflectivity factor η has to be computed. A three-dimensional cubic meshing with a mesh length $m = 125$ m is used. Due to the assumption of the uniformity of the storm vertical structure, only the horizontal plane has to be considered, so that the resolution volume is turned into a resolution surface. The plane is divided into elementary squares of side m. Doing this, the targets are decomposed into a sum of elementary squares, each of them being affected with a characteristic value according to the precipitation nature (hail, rain of 100, 80, 60, 40, 10 and 2 mm h^{-1}) of the region they belong to. Knowing the scatterer size distribution, the population of each resolution surface is determined so that it is possible to compute η and Z_e.

By the same quantization process, the attenuation undergone by the radar beam during the crossing of the target, that is,

$$a_T = 0.4343 \int_{D_{\min}}^{D_{\max}} N(D)Q(D)\, dD, \tag{6}$$

where Q is in cm^2, and other units as in (4), is computed for each resolution volume.

For gas attenuation, a pressure of 0.7 atm, a water vapor content of 10 g m^{-3}, and a temperature of 0°C were used (see Table 6).

In that way, for each resolution volume, the equivalent reflectivity factor Z_e is written as follows:

$$[Z_e(\text{dBZ})]_{\text{corrected}} = Z_e(\text{dBZ}) - 2(a_T - a_{H_2O} - a_{O_2}), \tag{7}$$

where 2 is for two ways, and a_{H_2O} and a_{O_2} are the at-

Unauthenticated | Downloaded 02/23/23 09:20 AM UTC

TABLE 4. One-way attenuation coefficients (dB km^{-1}) produced by uniform dry and coated ice spheres for an ice mass of 1 g m^{-3}. Symbols as in Table 3.

	Sphere diameter (D, cm)																	
	2.0			2.5			3.0			3.5			4.0					
τ (cm)	0.00	0.01	0.05	0.00	0.01	0.05	0.00	0.01	0.05	0.00	0.01	0.05	0.00	0.01	0.05			
λ (cm)																		
5.3	0.322	0.941	0.994	0.589	0.952	0.808	0.775	0.905	0.685	0.697	0.867	0.542	0.872	0.750	0.528			
10.7	0.021	0.079	0.375	0.043	0.110	0.737	0.074	0.154	0.890	0.113	0.215	0.718	0.156	0.304	0.614			

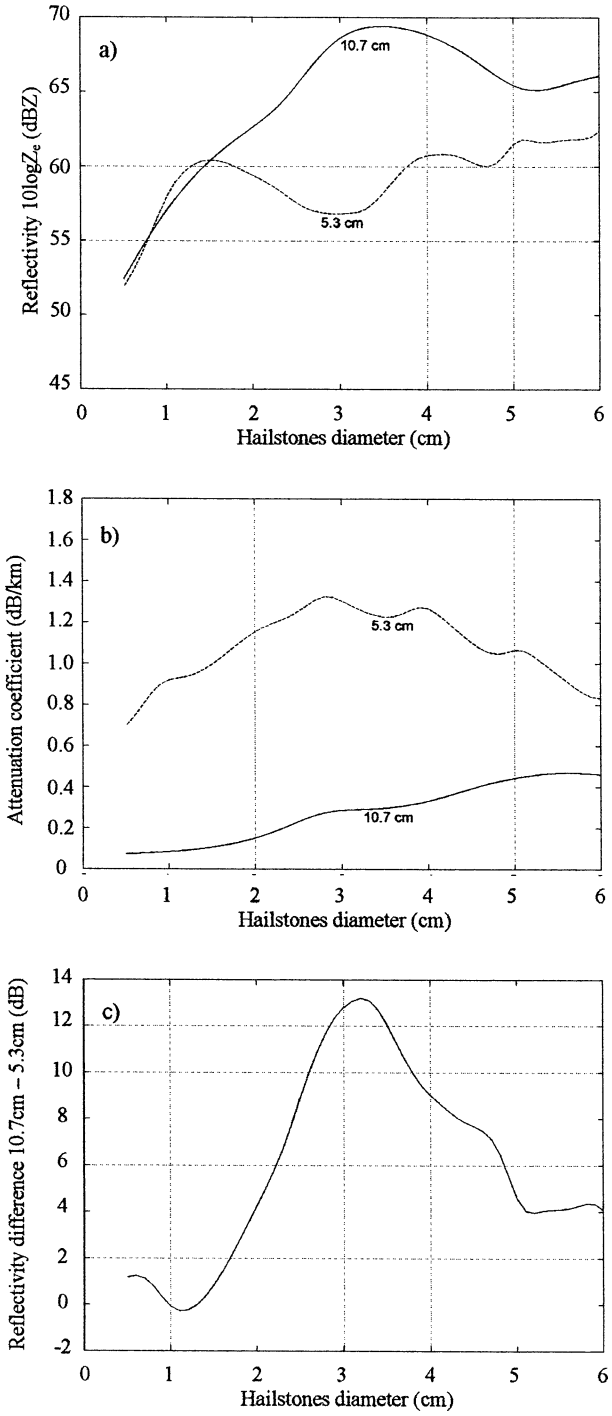

FIG. 5. (a) Reflectivity in dBZ and (b) two-way attenuation coefficient (in dB km^{-1}) as a function of the diameter D of the spherical hailstones for the modeled precipitation, that is, for a mixing made up of 50% of rain with rain rate of 100 mm h^{-1} and 50% of hailstones of diameter D. For the hailstones 50% are dry and 35% and 15% coated with a water shell of thickness 0.01 and 0.05 cm, respectively. The two wavelengths are 5.3 and 10.7 cm. (c) Reflectivity differences (attenuation included) between the 10.7- and 5.3-cm radars.

Unauthenticated | Downloaded 02/23/23 09:20 AM UTC

TABLE 5. Main technical characteristics of the radars used in the simulation.

	Radar 1	Radar 2
Wavelength (cm)	10.7 (S band)	5.3 (C band)
Peak power (kW)	700	250
Pulse repetition frequency (Hz)	250	330
Number of integrated pulses	23	30
Azimuthal speed (deg s^{-1})	5	5
Beamwidth (deg)	1.8	1.3
Range-gate length (m)	250	250
Number of gates averaged	2	2
Pulse duration (μs)	2	2

TABLE 6. Attenuation by water vapor and molecular oxygen in dB km^{-1} for one way at $T = 0°C$. In the simulation, the values of the pressure (P) and of the water vapor content (W) are equal to 0.7 atm and 10 g m^{-3}, respectively.

Wavelength (cm)	Water vapor	Molecular oxygen
10.7	$8 \times PW \times 10^{-5}$	$(1.19 \times P^2) \times 6.5 \times 10^{-3}$
5.3	$2.7 \times PW \times 10^{-4}$	$(1.19 \times P^2) \times 7.1 \times 10^{-3}$

tenuation coefficients by water vapor and molecular oxygen, respectively.

For a target at a distance d from the radar, the simulation is fully completed when the successive radar beams, separated by 0.5° in azimuth, have covered all the target extent. The simulated PPI radar scans thus obtained, in polar coordinates, are converted along a Cartesian grid, with a uniform pixel size of 1 km × 1 km, using an interpolation algorithm (e.g., Mohr and Vaughan 1979). Figure 6 shows the PPI images obtained by simulation for the two radars for $X = 100$ km. The reflectivity differences at 10.7 and 5.3 cm observed in case a result from the radar characteristics (3-dB beamwidth) but first and foremost from the attenuation differences undergone by the two wavelengths. Case b shows, as pointed out in Figs. 5a and 5c, the rapid increase of the reflectivity factor at 10.7 cm with respect to 5.3 cm. The spreading out in the direction perpendicular to the radar beam of the PPIs is obtained from simulation accounts for the azimuthal beam averaging. Moreover, the effect of attenuation generated by the target itself appears in the PPIs in the form of regions of low reflectivity values located mainly at the rear of the hail regions with respect to the radar location. This is particularly obvious at the short wavelength observations.

f. Hail detection: Dual-wavelength reflectivity ratio relevance and sensitivity

The efficiency of the DWHR method to detect hail is based on the rapid increase of the reflectivity factor difference $Z_{e10.7} - Z_{e5.3}$ in the presence of non-Rayleigh scatterers. The reflectivity factors that have to be considered are the ones presented in Fig. 5a. The $Z_{e10.7} - Z_{e5.3}$ difference starts to be appreciable for hailstone diameters larger than about 2 cm. As shown in Fig. 5b, the attenuation undergone by the radar beam during its way there and back across the target is far from being negligible. For each of the three kinds of targets considered in the simulations, that is, with circular, rectangular east–west and rectangular north–south horizontal cross sections, and the dual-wavelength reflectivity ratio can be computed as described in section 2. For each kind of target, the different compositions envisaged in the simulation are considered: the rain-only targets and the hail-bearing targets with hailstones of 2-, 2.5-, 3-, 3.5-, 4-, and 4.5-cm diameters, respectively. If $d_{10.7}$ and $d_{5.3}$ are the radial distances of observation from the target centroid located at $X = x$ km to the S- and the C-band radars, respectively, a dependency of the DWHR on the difference $d_{10.7}$–$d_{5.3}$ can be expected. More precisely, considering the 3-dB beamwidth of the 10.7-cm and of the 5.3-cm wavelength radar, $\theta_{10.7}$ and $\theta_{5.3}$, respectively, the dependency of DWHR on the difference of the beam width at distance $d_{10.7}$ and $d_{5.3}$ is of the form:

$$\text{DWHR} \propto f(d_{10.7}\theta_{10.7} - d_{5.3}\theta_{5.3}) = f(O_{10.7} - O_{5.3}),$$

where $O_{10.7}$ and $O_{5.3}$ are the azimutal width of the two radars at distance $d_{10.7}$ and $d_{5.3}$ respectively. Figure 7 displays the variation of DWHR as a function of the width difference for targets with rectangular north–south, rectangular east–west, and circular horizontal shape for ''rain'' and for hail-bearing targets producing hailstones of 2-, 2.5-, and 3-cm diameters. For the sake of clarity, the DWHR evolution of targets with 3.5-, 4-, and 4.5-cm hailstones are not shown in the figure. Their DWHR values are comprised between that of H2.5cm and H3cm, as suggested by Fig. 5c. In all the cases, 11 DWHR values are computed, which corresponds to the 11 successive target positions between $X = 0$ and $X = 200$ km considered in the simulations.

Figure 7 shows that, whatever the horizontal shape of the target, DWHR is linearly related to the width difference $O_{10.7}$–$O_{5.3}$. Moreover, the hail-bearing targets are clearly identifiable with respect to the rainy ones. This is especially true when the size of the hailstone population generates strong reflectivity differences between 10.7 and 5.3 cm as shown in Fig. 5c. Thus it is not surprising to observe relatively low DWHR values for hailstones of 2 cm. From Fig. 7, it is possible to determine the line that separates the rainy targets from those producing hailstones greater than 2.5 cm in diameter, whatever their horizontal shape. The equation of the line is of the form $y = A(O_{10.7} - O_{5.3}) + B$, with a slope A close to zero. This line does not permit us to distinguish the cells with hailstones of 2 cm size in the whole range of the width difference. It is due to the weak reflectivity differences at 10.7 and at 5.3 cm observed in Fig. 5c. It results in DWHR values close to those of the rainy targets or at least not sufficiently

Unauthenticated | Downloaded 02/23/23 09:20 AM UTC

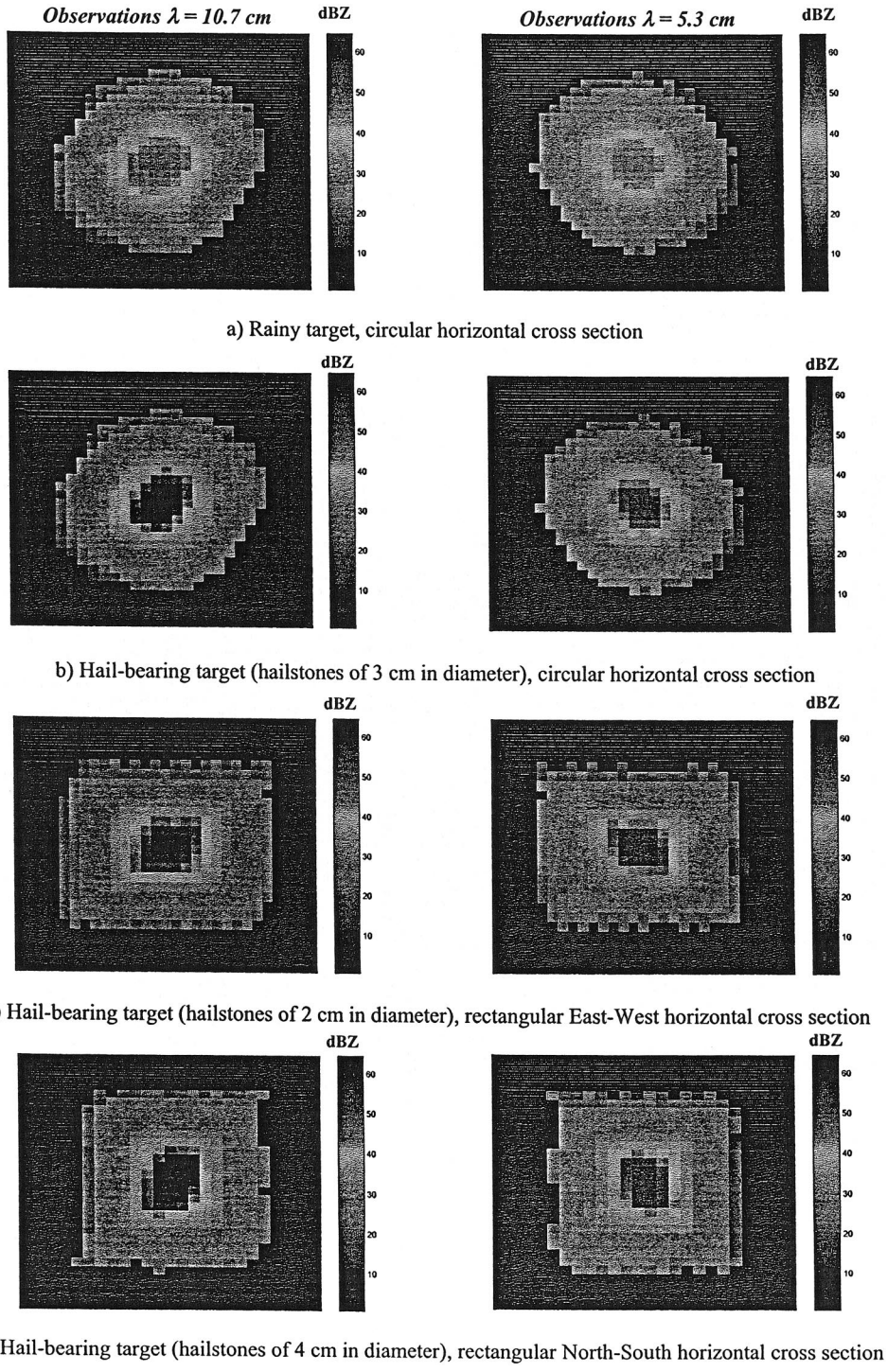

FIG. 6. PPI images obtained by simulation of radar observations at 10.7 and 5.3 cm for different kinds of targets with centroid located at $X = 100$ km from the 10.7-cm radar.

different to be detectable whatever the target horizontal profile is.

In the above simulations, the attenuation by precipitation over the radar–target path has not been considered. Of course, in the presence of a strong attenuation suffered, for example, for an observation through several storms lined up with the radar beam, the method fails. But such conditions are usually fortuitous and of short duration with respect to the lifetime of a hailstorm event over which the hail detection monitoring is performed.

Unauthenticated | Downloaded 02/23/23 09:20 AM UTC

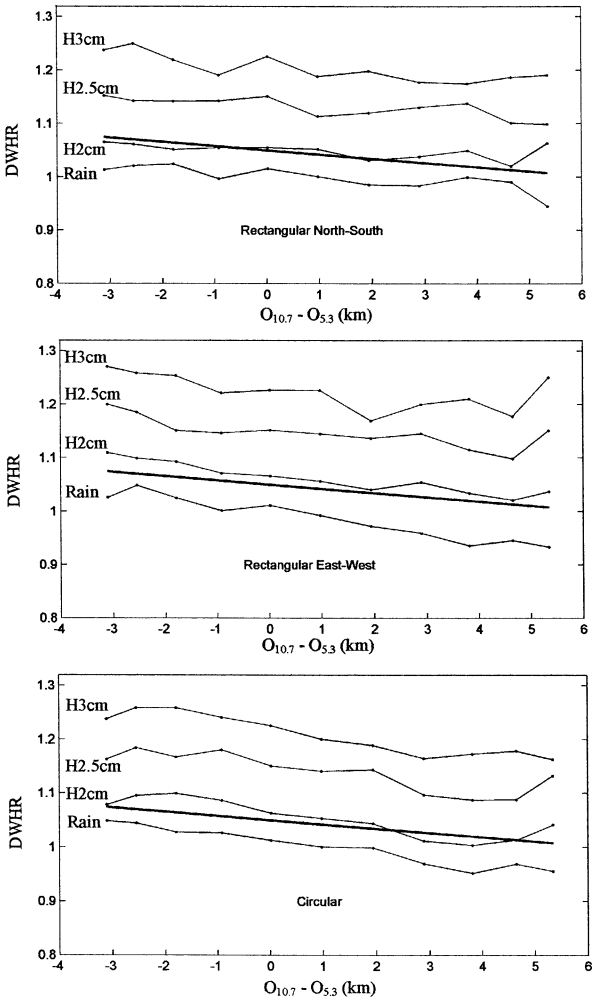

FIG. 7. Variation of the dual-wavelength reflectivity hail ratio DWHR as a function of the beamwidth difference for targets with rectangular north–south, rectangular east–west, and circular horizontal shape. The radar beam is assumed to not cross any attenuating medium (except gas) before reaching the target. ''Rain'' designates rainy targets, and H2cm, H2.5cm, and H3cm indicate hail-bearing targets with hailstones of 2-, 2.5-, and 3-cm diameter, respectively. The bold line separates the hail-bearing targets producing hailstones greater than 2.5 cm from the rainy ones whatever their horizontal profiles are and whatever the attenuation over the radar–target path. Its equation is DWHR $= -0.0079 \times (O_{10.7} - O_{5.3}) + 1.05$.

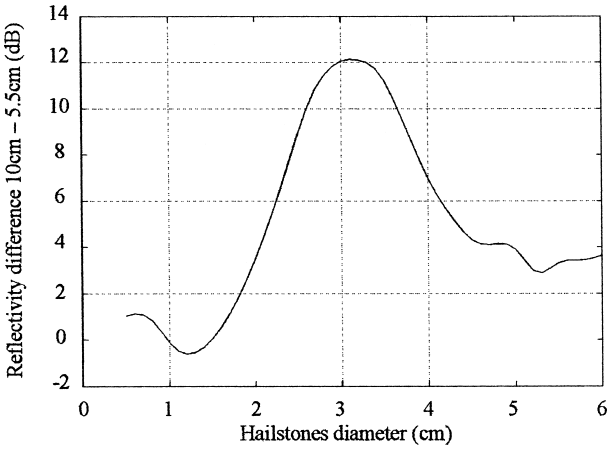

FIG. 8. Reflectivity differences (attenuation included) as a function of the diameter D of the spherical hailstones between a 10- and a 5.5-cm radar having a 3-dB beamwidth of 0.95° and 0.55°, respectively. The scattering volume composition is half rain with a rate of 100 mm h^{-1} and the other half hailstones with 50% dry and 35% and 15% coated with a water shell of thickness 0.01 and 0.05 cm, respectively.

In fact, the simulation shows that radar–target attenuation, even with relatively high values (up to 5 dB and 2 dB for 5.3- and 10.7-cm radar, respectively), does not significantly modify the results, because DWHR has the form of a hail/rain ratio. The DWHR variation is still linearly correlated with the width difference, while the curves are arranged according to their reflectivity differences shown in Fig. 5c. Therefore, the solution proposed is to define a sensitivity equation of DWHR as the equation of the line L separating the rainy targets from the hail-bearing ones, whatever their horizontal shape and whatever the attenuation applied on the radar beams before reaching the target. This equation is

$$\text{DWHR} = -0.0079(O_{10.7} - O_{5.3}) + 1.05. \quad (8)$$

As mentioned previously, the sensitivity equation of DWHR enables us to distinguish the targets that generate hailstones of diameter larger than 2.5 cm. Thus, the hail detection by dual-wavelength reflectivity ratio is really efficient in the case of hailstorms generating large hailstones.

The ability of the radars to detect hail areas is all the better as the azimuthal resolution increases. Simulations have been made using the characteristics of typical American radars [next-generation radar Weather Surveillance Radar-1998 Doppler (WSR-88D) and the terminal Doppler weather radar (TDWR)], that is, a 10-cm and a 5.5-cm wavelength radar with a 3-dB beamwidth equal to 0.95° and 0.55°, respectively. The reflectivity differences as a function of hailstone diameters are presented in Fig. 8. For sizes between 2 and 5 cm, the reflectivity difference is higher than 4 dB, with a peak of 12 dB for $D \sim 3$ cm. As previously, the dual-wavelength reflectivity ratio was computed. The results (Fig. 9) show that DWHR is still linearly correlated with the width difference but with slopes weaker than for the French radar network. This is due to the higher transverse resolution of the American radars that, in addition, allow the detection of hail regions of weaker horizontal extension than those identifiable with the Météo-France network. Finally, the sensitivity equation of DWHR in the case of the American radars is DWHR $= -0.0014(O_{10} - O_{5.3}) + 1.04$. As suggested by Fig. 8, targets that generate hailstones of 2.5 and 3.5 cm in

Unauthenticated | Downloaded 02/23/23 09:20 AM UTC

diameter have DWHR values between the ones of H4cm and H3cm.

4. Validation on real cases

To test the proposed DWHR method, three distinct hailstorm cases observed in southwestern France by the French meteorological radar network have been analyzed (Fig. 10). This radar network is made up of C- and S-band radars whose main characteristics are given in Table 5. For two of these cases, the data of the southwest hailpad network were available. This network is presented in Fig. 11. The hailmeters are extruded polystrene pads that are exposed to falling hailstones. After the hailfall, the impact dents are revealed by a black inking made with a roller and scanned for analysis (Dessens et al. 2001).

a. Data reduction and processing

The data were acquired in the form of PPIs every 5 min. Reflectivities were measured in contiguous range bins 500 m apart, over a circular area with a 256-km radius. The PPIs, in polar coordinates, were converted along a Cartesian grid, with an uniform pixel size of 1 km $\times$ 1 km, using an interpolation algorithm. For each cell constituting the rain field, the DWHR and the width difference were computed as described in section 2. The hail-bearing cells were identified according to the sensitivity equation (8) defined from the simulation for the French network.

b. Case of 21 April 1999

On 21 April 1999 an eastward-moving convective cold frontal line swept southwestern France. At about 1700 UTC, at the southern end of this line, a rainstorm became a supercell hailstorm causing heavy damage, with hailstones of about 3–5-cm diameter. The frontal line evolution, including the supercell hailstorm, was observed from birth to disappearance by the 5.3-cm radar, located at Toulouse, and by the 10.7-cm radar, situated at Nîmes (Fig. 10). This storm was the most severe and damaging event over a period of about 10 yr in the area of occurrence. Some aspects of this case are discussed in Féral and Sauvageot (2002).

Figure 12 illustrates the implementation of the proposed method to the reflectivity field observed by the two radars, and notably the definition of the precipitation areas. Figure 13 shows the DWHR variation computed for the supercell hailstorm from 1700 to 1840 UTC. The temporal variation of the DWHR displays an identifying signal for the supercell hailstorm. In the studied area, there were not any other DWHR signals of hail (i.e., larger than 2.5 cm in diameter) detected for that day. According to Fig. 13, the 21 April 1999 hailstorm seems to be composed of three hail events with hailstones greater than 2.5 cm in diameter. The first one occurs between 1705 and 1720 UTC, the second one between 1725 and 1800 UTC, and the third one between 1819 and 1827 UTC. The second one lasted 35 min with a DWHR maximum value of 115% toward 1740 UTC. This event seems to be the most intense. The three hail event durations coincide with the evolution of the supercell hailstorm, from its birth at around 1700 UTC to its disappearance at about 1835 UTC. Météo-France indicated hailfalls only for the zone swept by the supercell, with hailstones of about 3–5-cm diameter. No other hail was observed at the ground in the other parts of the convective field. All that leads to the conclusion that the DWHR seems to be, in this case, a rather good qualitative detector of the hail-bearing cells.

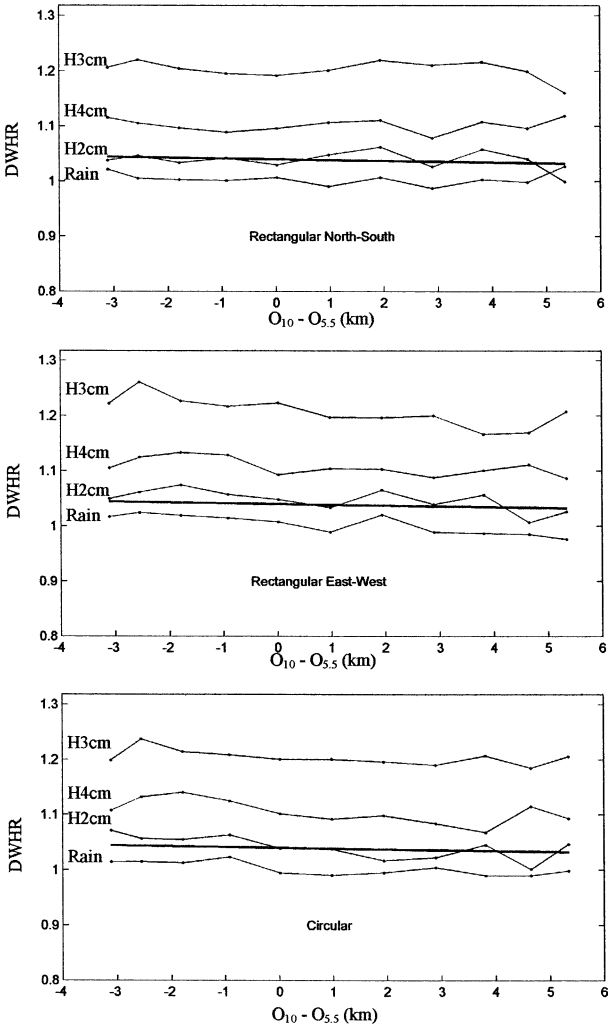

FIG. 9. Variation of the dual-wavelength reflectivity hail ratio DWHR as in Fig. 7 but now the radar beamwidths are 0.95° and 0.55° for the S and the C bands, respectively. ''Rain'' designates rainy targets, while H2cm, H3cm, and H4cm indicate hail-bearing targets with hailstones of 2-, 3-, and 4-cm diameter, respectively. The bold line separates the hail-bearing targets producing hailstones greater than 2.5 cm from the rainy ones whatever their horizontal profile and whatever the attenuation over the radar–target path. Its equation is DWHR $= -0.0014 \times (O_{10} - O_5) + 1.04$.

Unauthenticated | Downloaded 02/23/23 09:20 AM UTC

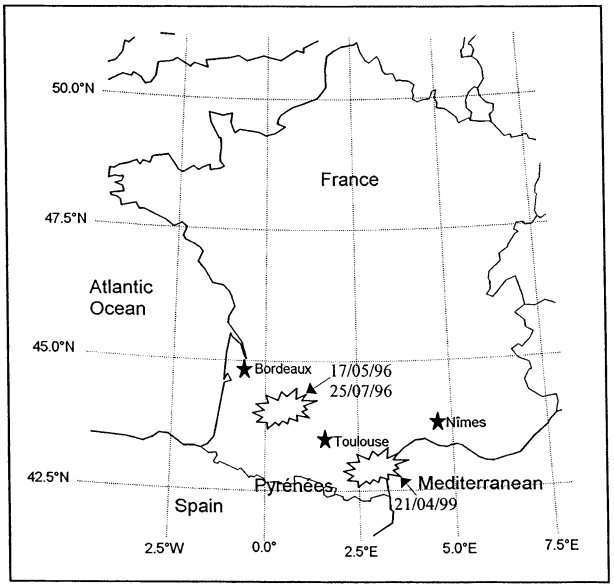

FIG. 10. Location of the hailstorms observed on 17 May 1996, 25 Jul 1996, and 21 Apr 1999 and of the radars involved in their observation (full starts). Bordeaux and Nîmes are S-band radars and Toulouse is a C-band radar.

c. Case of 25 July 1996

Since 22 July 1996, a Saharan southerly flow had been running over southwestern France. The temperature at the surface exceeded 30°C. On 25 July 1996, convective rain showers occurred. As for the 21 April 1999 case, at about 1700 UTC, an ordinary rainstorm over the Pyrénées Atlantiques burst into a supercell. Then it crossed the Landes along a southeast–northwest direction, with hailstones of about 3–4-cm diameter, until about 1915 UTC, when it began to regress. Written reports by ground observers of professional farming organizations noted severe and very localized hailfalls between 1715 and 1745 UTC over the Pyrénées Atlantiques. These hailfalls were not observed by the hailpad network (very scarce over the Pyrénées Atlantiques). The supercell hailstorm caused heavy damage across the Landes between 1745 and 1915 UTC. Figure 14a shows the time, location, and kinetic energy of hail im-

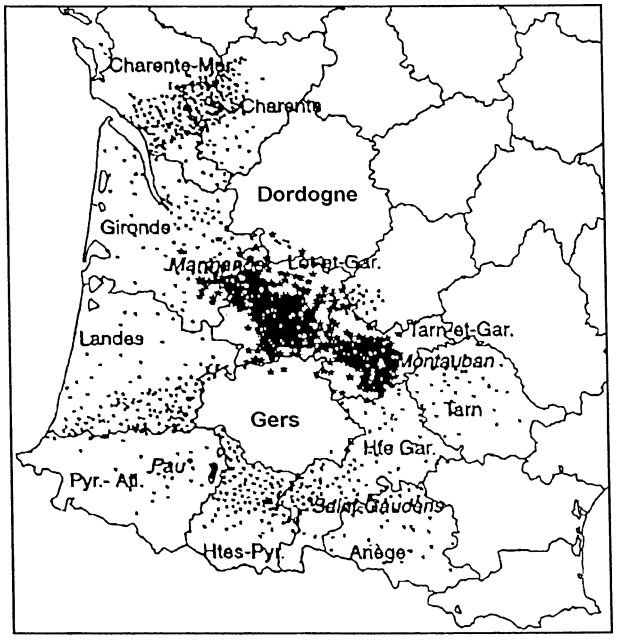

FIG. 11. The hailpad network in the southwest of France. The spots (●) and the stars (★) indicate the location of the stations managed by ANELFA (Association Nationale d'Etude et de Lutte contre les Fléaux Atmosphériques) and ACMG (Association Climatique de la Moyenne Garonne), respectively.

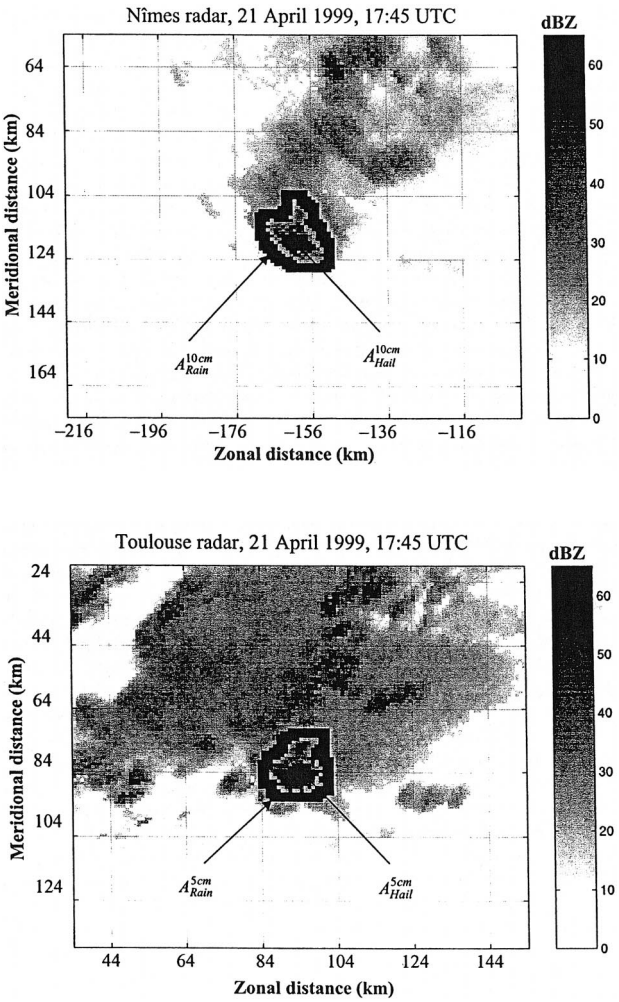

FIG. 12. (a) Radar reflectivity image from Nîmes radar observations of the 21 Apr 1999 supercell hailstorm at 1745 UTC. It shows the hail and rain areas as found by this technique. The size of the radar image is 512 km × 512 km. The supercell is about 200 km away from the radar. For clarity, the reflectivity of the $A_{\text{Rain}}^{10\text{cm}}$ and $A_{\text{Hail}}^{10\text{cm}}$ areas have been uniformly fixed to 65 dBZ. Regions with no signal are presented with a reflectivity value equals to 0 dBZ. (b) Same as (a) for Toulouse radar observation of the 21 Apr 1999 supercell hailstorm at 1745 UTC. The size of the radar image is 512 km × 512 km. The supercell is about 130 km away from the radar.

Unauthenticated | Downloaded 02/23/23 09:20 AM UTC

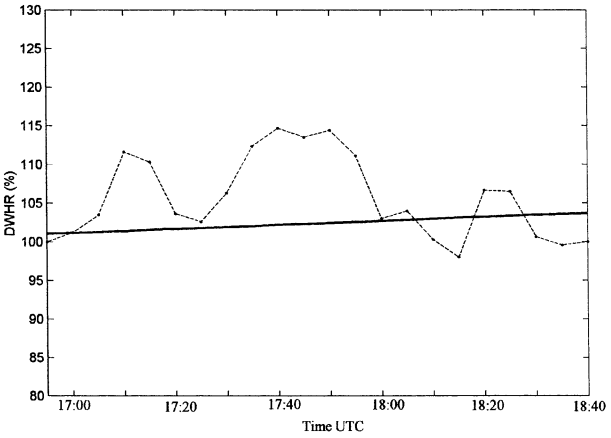

FIG. 13. Supercell dual-wavelength reflectivity hail ratio (DWHR) variation from 1700 to 1840 UTC on 21 Apr 1999. Every point corresponds to DWHR computed from simultaneous observations of the supercell by the radars of Toulouse and Nîmes each 5 min. The bold line stands for the sensitivity equation DWHR = $-0.0079 \times (O_{10} - O_5) + 1.05$ established from simulations for the French network.

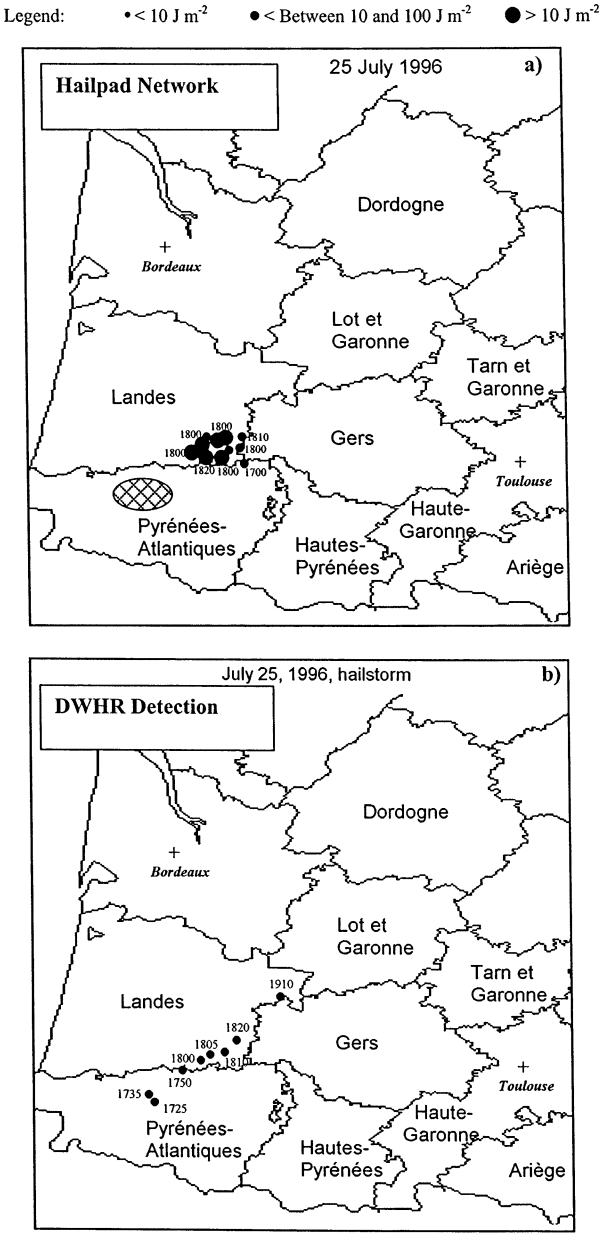

FIG. 14. (a) Time (UTC), location, and kinetic energy (J m^{-2}) of hail impacts measured by the hailpad network on 25 Jul 1996. The hatched area shows the location where ground observers reported severe hailfall between 1715 and 1745 UTC. (b) Hail-bearing cell locations according to the DWHR with the time (UTC) of their appearance for the 25 Jul 1996 hailstorm. There is no connection between the size of the spots and the kinetic energy of hail impacts.

pacts measured by the hailpad stations. The hailstorm was observed by the 5.3-cm wavelength radar of Toulouse and by the 10.7-cm wavelength radar of Bordeaux.

Figure 14b shows the centroid location and time of detection of areas identified by the DWHR as generating hailstones with diameters larger than 2.5 cm. The hail spots radar observed between 1725 and 1735 UTC over the Pyrénées Atlantiques are corroborated by the hailfall written reports by ground observers. The radar hail spots detected over the Landes between 1750 and 1820 UTC, with hailstones of 3–4-cm diameter, are in close correspondence with the hailpad network observations. Keeping in mind that the time of hailfalls given by the hailpad network is very approximate (because they are not automatically recorded), these hailfalls square well with the radar hail spots between 1715 and 1820 UTC. The DWHR computation indicates another hailfall at 1910 UTC in the northeastern part of the Landes, but the hailmeter network is not sufficiently dense in the corresponding area.

With negligible attenuation over the radar–target path and for a well-calibrated radar, the radar reflectivity factor at 10 cm, Z_{10}, can be considered as bearing information about the presence of hail, as recalled in section 1. In fact, when Z_{10} reaches values corresponding to improbable rain rate, it is reasonable to suspect the presence of hail. Using the standard Z–R relation recalled in section 2, a threshold of 60 dBZ corresponding to 223 mm h^{-1} can be considered. From the dual-wavelength radar results, among a population of 54 storm cells, 24 match with the spatial agreement criterion ($D_{IB} < 5$ km and $P_{SC} > 50\%$). Among these, eight are identified as being hail-bearing cells according to the sensitivity equation. Here, all the storm cells that offer a maximum of reflectivity equal to or greater than 60 dBZ are classified as hail-bearing cells by the hail-detection algorithm.

d. Case of 17 May 1996

On 17 May 1996, a low pressure zone over the near Atlantic directed a rapid southwesterly flow over southwestern France where, in the late afternoon, hailstorms

Unauthenticated | Downloaded 02/23/23 09:20 AM UTC

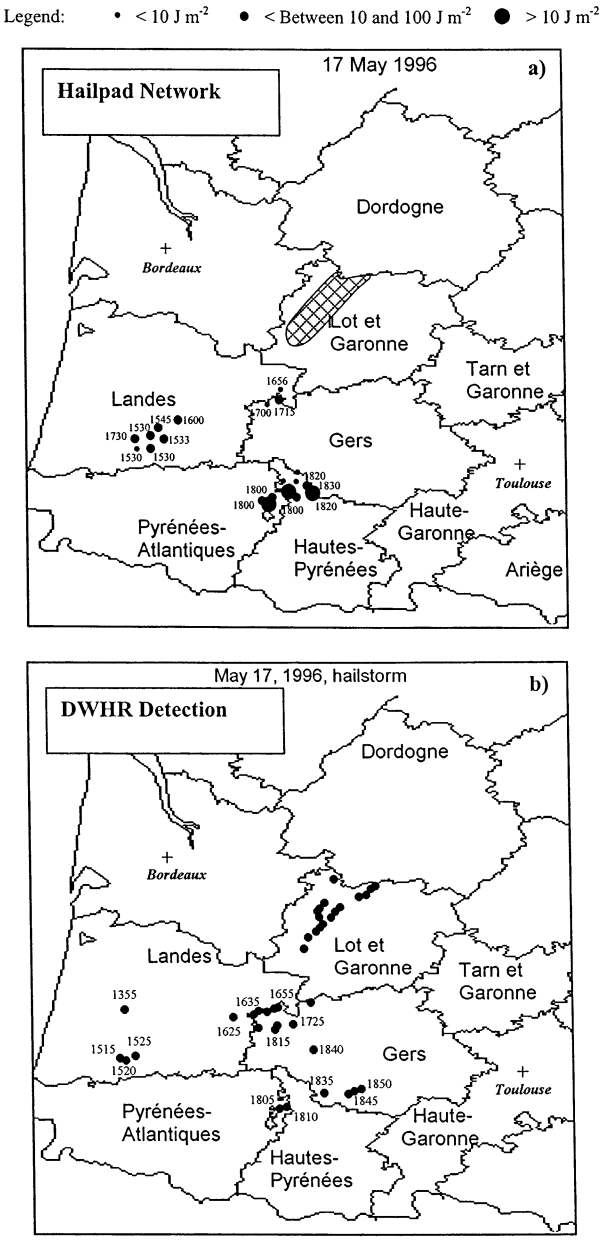

FIG. 15. (a) Time (UTC), location, and kinetic energy (J m^{-2}) of hail impacts measured by the hailpad network on 17 May 1996. The hatched area shows the limit of the region where hailfalls were observed over Lot-et-Garonne (the pinpoint data were not available from the Lot-et-Garonne network). (b) Hail-bearing cell locations according to the DWHR. There is no connection between the size of the spots and the kinetic energy of hail impacts.

were observed. Figure 15a shows the time, location, and kinetic energy of hail impacts recorded by the hailpad network. The rain field was observed by the radar of Toulouse and the radar of Bordeaux.

Figure 15b shows the rain cell centroid locations the radar identified as being hail-bearing cells, generating hailstones with diameters larger than 2.5 cm. From the DWHR results, among a population of 439 storm cells, 310 match with the spatial agreement criterion ($D_{IB} <$ 5 km and $P_{SC} > 50\%$). Among these, 55 are hail-bearing cells. Thus, for the 17 May 1996 case, 17% of the storm cells are hail-bearing cells. Moreover, all the storm cells having a maximum S-band reflectivity superior or equal to 60 dB*Z* are classified as hail-bearing cells, except one. Its maximum reflectivity is 60 and 59 dB*Z* for the S- and the C-band radars, respectively. The difference is weak and leads to the assumption that this cell contains hailstones with diameter smaller than 2.5 cm. If a rather good spatiotemporal agreement with respect to the hailfalls recorded by the hailpad network can be observed, the DWHR indicates other hailfalls, over the Landes and the Gers. One can account for these differences by considering the hailpad network in Fig. 11. It shows that the Gers has no hailpad and that the network in the western part of the Landes is not dense.

5. Conclusions

A new dual-wavelength radar method for hail detection from an S-band and a C-band radar, located far from each other, has been proposed. This method uses the reflectivity difference of large hail at S and C bands, due to the non-Rayleigh scattering effects.

From the data of each radar, the ratio of the area-averaged reflectivity factor of the suspected hail core to that of the surrounding rain is computed. Forming these ratios enables us to obtain two terms weakly dependent on the radar technical parameters and on the attenuation over the radar–target path, measuring for each wavelength the relative reflectivity of hail with respect to rain. The ratio of the relative reflectivity of the hail-suspected cell for the S-band radar to that for the C-band radar forms the dual-wavelength hail ratio (DWHR). For rain only, that is, for a Rayleigh target, DWHR is around one, while in the presence of large hail, that is, non-Rayleigh scatterers, DWHR is larger than one. The present method will be termed the ''DWHR method.''

The sensitivity of the DWHR method to the shape, size, and structure of the rain cells, with respect to the shape and size of the pulse volume, that is, the radar–target distance, was analyzed through a numerical study of backscattering and attenuation by dry and wet hailstones and through a simulation of the method. The reflectivity factor difference for S and C bands becomes significant for hailstone diameters larger than about 2 cm, and peaks around 3 cm, then decreases for larger sizes. The DWHR method is found not to be affected by the shape or by the observing distance (provided that the convective field remains correctly sensed by the radars) up to 200 km of distance, in the simulation conditions. A qualitative hail signal is clearly obtained from DWHR for hailstone diameters larger than 2.5 cm, with a peak for hailstones around 3 cm.

DWHR is found to be linearly dependent on the difference between the azimuthal widths of the S-band and

Unauthenticated | Downloaded 02/23/23 09:20 AM UTC

the C-band radar, that is, $(O_{10.7} - O_{5.3})$. An ''equation of sensitivity'' relating the sensitivity threshold of DWHR linearly to the $(O_{10.7} - O_{5.3})$ difference was written. The DWHR variation with respect to $(O_{10.7} - O_{5.3})$ remains parallel to the sensitivity curve, and DWHR is not degraded by the relative radar–target distance, with respect to the S- and C-band radars. Computations were performed using the characteristics of two radars of the French operational network with 3-dB beamwidth 1.8° and 1.3° for S and C bands, respectively, and for the American radars WSR-88D and TDWR having a 3-dB beamwidth of 0.95 and 0.55° for S and C bands, respectively. For this last case, DWHR is found to be almost independent from $(O_{10} - O_{5.5})$.

The DWHR method was then tested on three field cases observed with S- and C-band radars of the French operational network more than 200 km apart from each other. The DWHR detection signal was compared to the hail reports at the ground provided by professional observers, and by a hailpad network. Results for hailstorms located up to 200 km from the radars show a very good qualitative agreement between the DWHR hail detection and the ground observations. It is suggested in conclusion that the DWHR method has a potential for hail detection.

Of course the DWHR approach described in the present paper can also be used with a dual-wavelength radar (i.e., when the two radars are collocated).

Acknowledgments. The authors are very grateful to Météo-France, for providing free of charge radar data from Bordeaux, Nîmes, and Toulouse, and to the ANELFA (Association Nationale d'Etudes et de Lutte contre les Fléaux Atmosphériques) and ACMG (Association Climatique de la Moyenne Garonne) for providing the data of their hailpad network free of charge.

REFERENCES

Aden, A. L., and M. Kerker, 1951: Scattering of electromagnetic waves from two concentric spheres. *J. Appl. Phys.,* **22,** 1242–1246.

Atlas, D., 1954: The estimation of cloud parameters by radar. *J. Meteor.*, **11,** 309–317.

——, Ed.,1990: *Radar in Meteorology.* Amer. Meteor. Soc., 806 pp.

——, and F. H. Ludlam, 1961: Multi-wavelength radar reflectivity of hailstorms. *Quart. J. Roy. Meteor. Soc.*, **87,** 523–534.

——, and C. W. Ulbrich, 1974: The physical basis for attenuation rainfall relationships and the measurement of rainfall parameters by combined attenuation and radar methods. *J. Rech. Atmos.*, **8,** 275–298.

Battan, L. J., 1971: Radar attenuation by wet ice spheres. *J. Appl. Meteor.,* **10,** 247–252.

Bringi, V. N., J. Vivekanandan, and J. D. Tuttle, 1986: Multiparameter radar measurements in Colorado convective storms. Part II: Hail detection studies. *J. Atmos. Sci.,* **43,** 2564–2577.

Browning, K. A., and Coauthors, 1976: Structure of an evolving hailstorm. Part V: Synthesis and implications for hail growth and hail suppression. *Mon. Wea. Rev.,* **104,** 603–610.

Byers, H. R., and R. R. Braham Jr., 1949: *The Thunderstorm.* U.S. Dept. of Commerce, 287 pp.

Changnon, S. A., 1970: Hailstreaks. *J. Atmos. Sci.,* **27,** 109–205.

Deirmendjian, D., 1969: *Electromagnetic Scattering on Spherical Polydispersions.* Elsevier, 290 pp.

Dessens, J., 1986: Hail in southwestern France: Hailfall characteristics and hailstorm environment. *J. Climate Appl. Meteor.*, **25,** 35–47.

——, R. Fraile, V. Pont, and J. L. Sanchez, 2001: Day-of-the-week variability of hail in southwestern France. *Atmos. Res.,* **59,** 63–76.

Eccles, P. J., and E. A. Mueller, 1971: X-band attenuation and liquid water content estimation by dual-wavelength radar. *J. Appl. Meteor.,* **10,** 1252–1259.

——, and D. Atlas, 1973: A dual wavelength radar hail detector. *J. Appl. Meteor.,* **12,** 847–854.

Féral, L., and H. Sauvageot, 2002: Fractal identification of supercell storms. *Geophys. Res. Lett.,* **29** (14), 1686, doi: 10.1029/2002GL015260.

Gosset, M., and H. Sauvageot, 1992: A dual-wavelength method of ice-water characterization in mixed-phase clouds. *J. Atmos. Oceanic Technol.*, **9,** 538–547.

Hogan, R. J., A. J. Illingworth, and H. Sauvageot, 2000: Measuring crystal size in cirrus using 35- and 94-GHz radars. *J. Atmos. Oceanic Technol.,* **17,** 27–37.

Illingworth, A. J., J. W. F. Goddard, and S. M. Cherry, 1987: Polarization radar studies of precipitation development in convective storms. *Quart. J. Roy. Meteor. Soc.,* **113,** 469–489.

Jameson, A. R., and R. C. Srivastava, 1978: Dual-wavelength Doppler radar observations of a hail at vertical incidence. *J. Appl. Meteor.,* **17,** 1694–1703.

Kennedy, P. C., A. Rutledge, W. A. Petersen, and V. N. Bringi, 2001: Polarimetric radar observations of hail formation. *J. Appl. Meteor.,* **40,** 1347–1366.

Kessler, E., 1983: *Thunderstorms: A Social, Scientific and Technological Documentary.* University of Oklahoma Press, 411 pp.

Marshall, J. S., and W. M. K. Palmer, 1948: The distribution of raindrops with size. *J. Meteor.*, **5,** 165–166.

Mohr, C. G., and R. L. Vaughan, 1979: An economical procedure for Cartesian interpolation and display of reflectivity factor data in three-dimensional space. *J. Appl. Meteor.,* **18,** 661–670.

Ray, P. S., 1972: Broadband complex refractive indices of ice and water. *Appl. Opt.,* **11,** 1836–1844.

Rinehart, R. E., and J. D. Tuttle, 1982: Antenna beam patterns and dual-wavelength processing. *J. Appl. Meteor.,* **21,** 1865–1880.

Sauvageot, H., 1992: *Radar Meteorology.* Artech House, 366 pp.

——, 1996: Polarimetric radar at attenuated wavelength as a hydrological sensor. *J. Atmos. Oceanic Technol.,* **13,** 630–637.

Tuttle, J. D., and R. E. Rinehart, 1983: Attenuation correction in dual-wavelength analyses. *J. Climate Appl. Meteor.,* **22,** 1914–1921.

Vinet, F., 2001: Climatology of hail in France. *Atmos. Res.,* **56,** 309–323.

Vivekanandan, J., B. Martner, M. K. Politovich, and G. Zhang, 1999: Retrieval of atmospheric liquid and ice characteristics using dual-wavelength radar observations. *IEEE Trans. Geosci. Remote Sens.,* **37,** 2325–2334.

Young, K. C., 1993: *Microphysical Processes in Clouds.* Oxford University Press, 427 pp.

Unauthenticated | Downloaded 02/23/23 09:20 AM UTC